Study of di-electrons with MPD at NICA

V. Vasendina[*], V. Jejer, S. Lobastov, I. Tyapkin, and A. Zinchenko

VBLHEP JINR, Dubna, Russia

G. Musulmanbekov

LIT JINR, Dubna, Russia

Abstract

One of the main tasks of NICA/MPD physics program is a study of low mass vector mesons ρ, ω, ϕ by measurements of their dileptonic decay channels. In this paper the current status of dielectron simulations in MPD is presented and the detector performance for such measurements is discussed.

[*]vasveron@mail.ru

1 Introduction

At sufficiently high temperature and/or baryon density, which could be realized in heavy ion collisions, the existence of new phases of matter, the Quark-Gluon Plasma (QGP) is predicted. At these temperatures and densities the excitation of the QCD vacuum can lead to the restoration of chiral symmetry and deconfinement of color charges. These phenomena are the goals for the project Nuclotron-based Ion Collider fAcility (NICA) which is being developed at JINR, Dubna. The project includes design and construction of a heavy ion collider for the energy range $\sqrt{s}$ = 4-11 GeV, and the Multi-Purpose Detector (MPD) which is optimized for the study of properties of hot and dense matter in heavy-ion collisions [1]. It is expected that this energy region will allow analyzing the highest baryonic density under laboratory conditions.

The important observable for chiral symmetry restoration is the modification of the properties of vector mesons at high baryon density. Their in-medium properties can be studied by measuring the dileptonic decay channels. Dileptons represent a penetrating probe of the hot and dense nuclear matter created in heavy ion collisions. Since dileptons interact only electromagnetically, their mean free path is large compared to the size of the system formed in these collisions. They are thus not distorted by final state interactions and once produced can escape unaffected the interaction region, carrying to the detectors information about the conditions and properties of the medium at the time of their creation. Analyzing invariant mass dilepton spectra, one can extract information on the modifications induced by the medium on specific properties of the vector meson, such as its mass and/or its width.

Low-mass dileptons in nuclear collisions were measured in three different energy ranges: 1-2 AGeV at the DLS (BEVALAC) [2] and HADES (GSI) [3], 40 and 158 AGeV at the CERN SPS [4–8] as well as $\sqrt{s_{NN}}$ = 200 GeV at RHIC [9,10]. All experiments observed an enhanced production of dileptons over a very broad invariant mass range of m_{ll} from $\sim$200 MeV/c^2 up to $\sim$700 MeV/c^2. There are no measurements performed in the energy range E_{Lab} = 2-40 AGeV. It is very important to cover this energy gap, since an enhancement of low-mass dileptons are observed both at low (BEVALAC and HADES) and high (SPS) energies studied, and it is not clear that the enhancement reflects the same physics in all cases.

The measurement of dileptons yield is rather complicated. There are two main difficulties. The first one is the huge combinatorial background of uncorrelated lepton pairs. It arises from the fact that, since single leptons do not preserve any information about their parent particle, all leptons are paired with all anti-leptons in the same event to form the invariant mass spectrum. This background therefore depends quadratically on the particle multiplicity and strongly increases as the coverage moves to low-p_T leptons. In the measurement of e^+e^- pairs, the combinatorial background mainly comes from π^0 Dalitz decays and conversions. The second difficulty is the physics background. Dileptons can be emitted by a variety of sources and therefore before claiming observation of any new effect, it is mandatory to have a thorough understanding of the expected contribution from all known sources. Therefore, one of the main tasks of NICA/MPD program, is reconstruction of low mass vector mesons ρ, ω, ϕ by the measurements of their dileptonic decay channels. In this article we present the status of simulation of dielectron measurements and low mass vector meson reconstruction performance in MPD.

2 Detector geometry

The detailed description of the MPD geometry can be found in Ref. [1]. The present analysis is based on the detectors covering the mid-rapidity region: the main tracker Time Projection Chamber (TPC), barrel Time-Of-Flight system (TOF) and barrel ElectroMagnetic Calorimeter (EMC). Another relevant detector element is the beam pipe which was taken to be made of beryllium with a wall thickness of 1 mm. The overall detector material budget can be seen in Fig. 1.

3 Detector performance

3.1 Track reconstruction

Track finding efficiency in TPC for electrons and pions is shown in Fig. 2 as a function of track transverse momentum. The efficiency of track matching with TOF can be seen there as well. The plateau value of $\sim90\%$ of matching efficiency is due to the gaps between TOF modules in azimuthal direction [1]. The transverse momentum resolution as a function of p_T can be seen in Fig. 3.

3.2 Particle identification

Particle identification is based on combination of measurements from three detector subsystems in order to achieve the best results: dE/dx in TPC, time-of-flight in TOF and EMC and E/p in EMC. The identification method used is as follows: for TPC tracks with a good match in TOF or EMC the time-of-flight measurement and momentum give an estimate of the particle velocity β. When combined with dE/dx in TPC, the obtained separation of electrons from other species is quite good as can be seen in Fig. 4. In addition, if the track reaches EMC, the calorimeter signal for a given momentum provides another particle identification criterion (Figs. 5,6). For tracks without a match in TOF or EMC, only a dE/dx-cut is applied in some momentum intervals (Fig. 7). The resulting electron selection efficiency, i.e. probability of a true positive identification of reconstructed electrons, is shown in Fig. 8 as a function of electron momentum, and the overall hadron rejection factor achieved is ~3200 (Fig. 9).

4 Event generators

The study of dielectron production in central (0-3 fm) gold-gold collisions at 7 AGeV was performed using Pluto generator [11] which produced a cocktail of hadrons decaying into electron-positron or Dalitz electron-positron pairs. The multiplicity of such electron sources was taken from the UrQMD generator [12]. As can be seen in Figs. 10, 11, Pluto quite well reproduces main parameters of electron sources (p_t and y). For the full simulation, the Pluto output was mixed with UrQMD generated events, where tracks from Dalitz decays of π^0 and η were excluded to avoid double counting.

5 Analysis procedure

5.1 Track selection

To ensure track quality the following cuts were applied: $|\eta| < 1.2$, number of TPC hits on track not less than 20 and the track should come from the primary vertex, i.e. the distances of the closest approach to the primary vertex (in transverse and longitudinal directions) should be below 3σ of the respective distributions for primary tracks.

5.2 Event samples

Since the full data analysis chain includes transport of particles through the detector, track reconstruction and particle identification procedures and quite time consuming, at present we used somewhat simplified approach where only a relatively small number (10 thousand) of central gold-gold collisions from the UrQMD generator (which give a background contribution) was simulated and then mixed with much larger signal event samples from Pluto (20 million, corresponding to the running time of $\sim$18 hours at 6 kHz NICA collision rate). The event mixing procedure was realized as follows: the UrQMD event sample was fully processed and the tracks remaining after the electron identification criteria and some extra acceptance cuts (see below) were stored as a common track pool. Then, for each Pluto event, a random track selection from this pool was done with the requirement to reproduce the residual UrQMD track multiplicity distribution (Fig. 14).

5.3 Background suppression

Since the particle identification provides the high hadron rejection factor, the main source of the remaining background is photon conversions in the detector material. The conversion pairs can be rejected by a topological cut, making use of the fact that the electron-positron pair is produced with almost zero opening angle. In the magnetic field the particle trajectories are deflected in such a way, that the plane formed by the electron and positron momenta is oriented mainly orthogonal to the magnetic field direction (the normal to the plane is mostly parallel to the magnetic field) [9]. We have complemented this value by the radial position of the production point of the di-electron and applied a 2-dimensional cut (Fig. 12). This cut removes the majority of the conversion pairs. However, a sizeable fraction of conversion products remained due to the fact that in some cases only one electron or positron was reconstructed. To further suppress those, the low-momentum cut can be applied (Fig. 13). A high-p cut (2 GeV/c) was also applied to decrease the residual hadron (mostly proton) contamination. The final background multiplicity distribution from UrQMD is shown in Fig. 14 as compared with the signal one (Pluto). One can see, that the residual hadron contamination is $\sim$1.5%.

6 Results and discussion

The results presented below have been obtained after a so-called "π^0"-rejection had been applied. The essence of this procedure consists in the following: if in the event there is an electron-positron combination with the invariant mass below 0.2 GeV/c^2 both tracks are excluded from further track combinations as coming from a π^0 Dalitz decay [5]. It was observed

that this assumption was indeed most of the time correct and helped to improve the signal-to-background ratio. Another selection cut, $\sqrt{p_{e^+}p_{e^-}} > 0.3$ GeV/c [13], was also found to be useful.

Fig. 15 shows invariant mass distributions of electron-positron pairs and signal-to-background ratios in invariant mass bins for two values of pseudorapidity cuts, $|\eta| < 0.5$ and 1.0. There is an apparent advantage (in terms of the signal-to-background ratio) of using a smaller detector pseudorapidity acceptance due to the fact, that the signal statistics depends linearly on the acceptance while the background contribution scales quadratically. However, the acceptance restriction causes a loss of signal, which can be partially reduced if a slightly different constrain is used, i.e. a pair is formed only if two tracks lie within some interval of pseudorapidity (Table 1). One can see also that the detector originated background (mostly due to conversion electrons) presents quite a significant fraction and this fact justifies further efforts to reduce it. In particular, a larger radius of the beam pipe would provide better conditions for rejecting unpaired conversion electrons produced inside the pipe wall due to their larger overall distance of the closest approach to the primary vertex ("primary vertex origin"-cut), and this improvement was indeed observed (see Table 1). The obtained results on signal-to-background values are shown in Fig. 16 along with the published data from other experiments.

7 Plans

Since it is planned to have an extended MPD geometry available for dielectron studies (up to $|\eta| < 2.0$) it will be necessary to evaluate the impact of the extended configuration on the dielectron physics, i.e. the full analysis chain should be exercised for the extended setup, including track reconstruction and particle identification in the endcap region.

The installation of the inner tracking system made of silicon detectors would also affect the detector performance due to additional amount of material and, on the other hand, better determination of track parameters near the interaction region.

The experimentally observed enhancement of spectra of di-electrons in the invariant mass region of 0.2 - 0.6 GeV/c^2 needs new mechanisms of vector meson formation in a dense nuclear matter for its explanation, e.g. as proposed and implemented in the event generators QGSM [14] and HSD [15], which are planned to be utilized in order to obtain better estimates of the signal-to-background ratio.

8 Acknowledgements

References

[1] http://nica.jinr.ru/files/CDR_MPD/MPD_CDR_en.pdf

[2] R.J. Porter *et al.* (DLS Collaboration), Phys. Rev. Lett. **79**, 1229 (1997).

[3] A. Rustamov *et al.* (HADES Collaboration), Int. Jour. Mod. Phys. A **26** 384-389 (2011).

[4] G. Agakichiev *et al.* (CERES Collaboration), Phys. Rev. Lett. **75**, 1272-1275 (1995).

[5] D. Adamova *et al.* (CERES Collaboration), Phys. Rev. Lett. **91**, 042301-1 (2003).

[6] G. Agakichiev *et al.* (CERES Collaboration), Eur. Phys. J. C **41**, 475-513 (2005).

[7] D. Adamova *et al.* (CERES Collaboration), Phys. Lett. **666**, 425-429 (2008).

[8] R. Arnaldi *et al.* (NA60 Collaboration), Phys. Rev. Lett. **96**, 162302 (2006).

[9] A. Adare *et al.* (PHENIX Collaboration), Phys. Rev. C **81**, 034911 (2010).

[10] F. Geurts, Di-Lepton Physics Program at STAR, Quark Matter 2012 Conference.

[11] I. Frohlich *et al.*, arXiv:0708.2382v2 [nucl-ex].

[12] http://urqmd.org/

[13] T. Galatyuk, Phd thesis, Johann Wolfgang Goethe Universität, Frankfurt am Main, Germany (2009).

[14] L.V. Bravina *et al.*, Nucl. Phys. A **566**, 461c (1994).

[15] W. Cassing, E.L. Bratkovskaya, and S. Juchem, Nucl. Phys. A **674**, 249 (2000).

[16] T. Galatyuk, Exploring phase diagram of matter with virtual photons, http://www-aix.gsi.de/conferences/emmi/epd2012/.

Detector acceptance $|\eta|$	$|\Delta\eta_{e^+e^-}|$	Signal	S/B, %	S/B, % ($R_{pipe} = 20$ cm)
< 1.0	-	13025	6.8	10.7
< 0.5	-	3754	10.1	12.7
< 1.2	< 1.0	14198	8.2	13.2
< 1.2	< 0.5	8616	9.4	15.7
< 1.2	< 0.25	4531	9.6	16.8

Table 1: Number of selected signal dielectron pairs and signal-to-background ratio for different detector pseudorapidity acceptances $|\eta|$ and different cuts on e^+e^- pseudorapidity distance $|\Delta\eta_{e^+e^-}|$. The last column shows the signal-to-background ratio for the setup with the beam pipe radius of 20 cm.
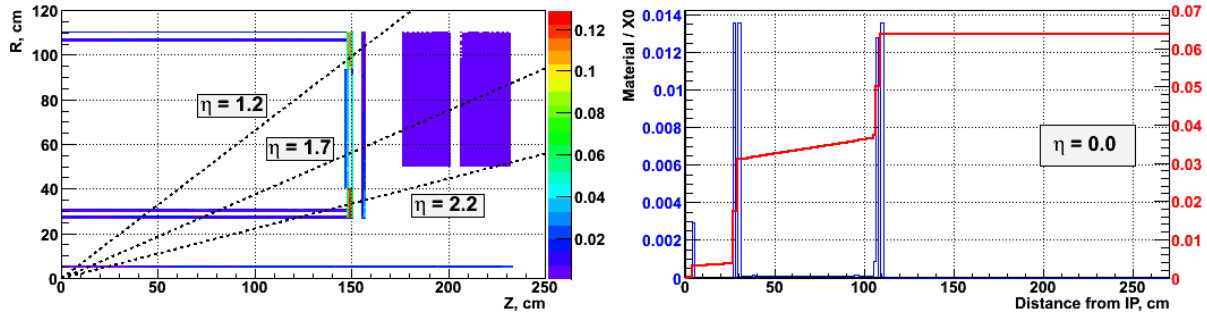
Figure 1: Left) detector material budget (in units of radiation length $X0$) vs Z and R; right) detector material vs distance from the beam line at $\eta =0$ (the left and right scales are for the differential and cumulative distributions, respectively).
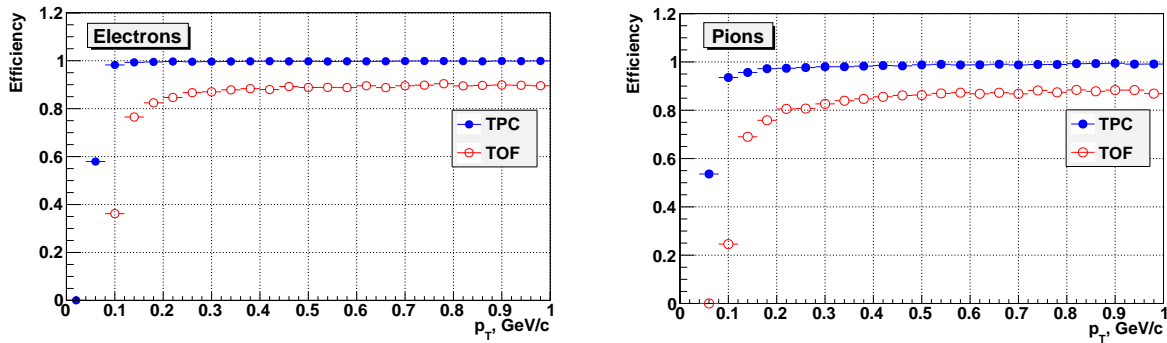
Figure 2: Tracks reconstruction and TOF matching efficiencies as functions of track p_T for electrons (left) and pions (right).
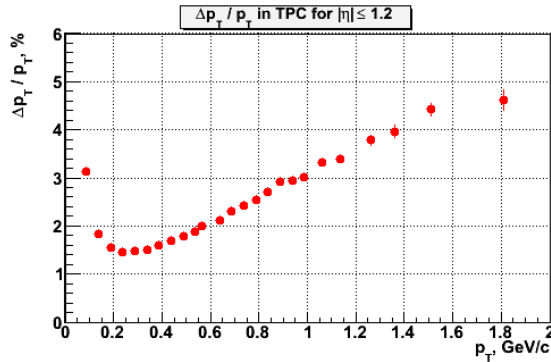
Figure 3: Relative transverse momentum resolution versus p_T for tracks with $|\eta| <1.2$ reconstructed in TPC.
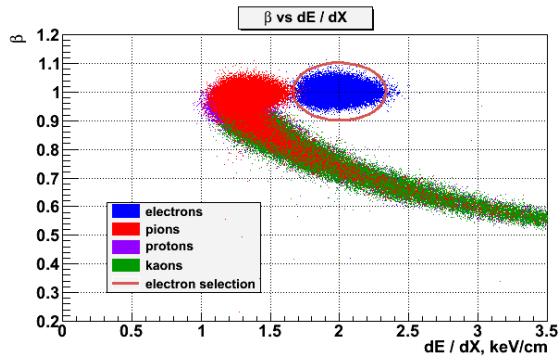
Figure 4: Reconstructed track velocity versus dE/dx for different particle species.
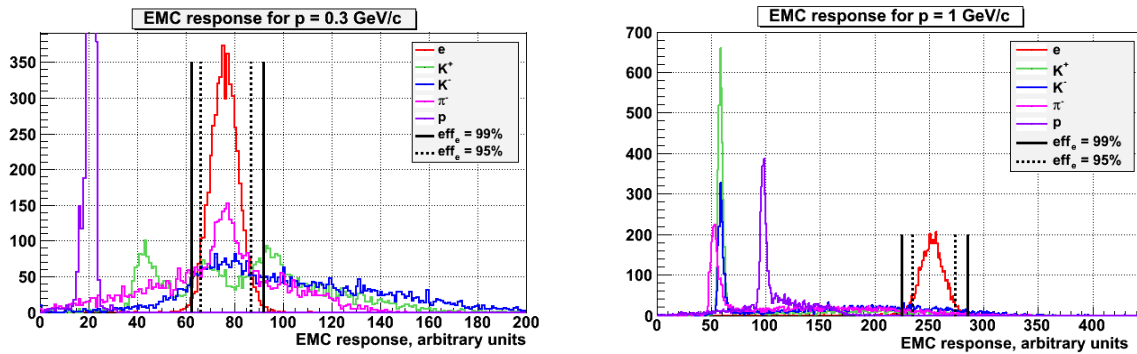
Figure 5: EMC response for different particle species with momentum of 0.3 GeV/c (left) and 1.0 GeV/c (right).
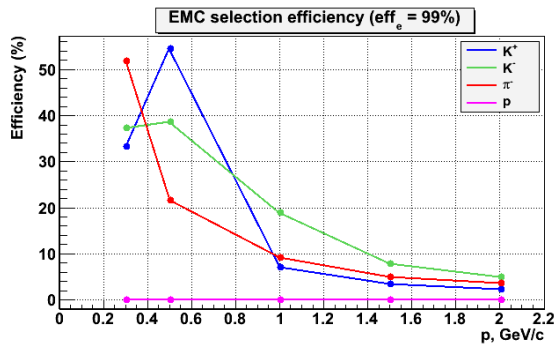
Figure 6: EMC hadron misidentification efficiency (probability to identify a hadron as an electron) versus momentum for different particle species with 99% electron efficiency.
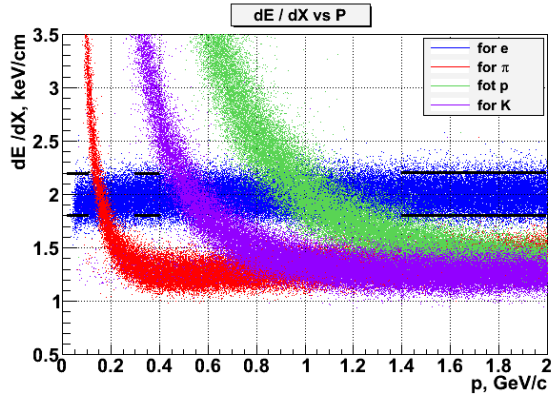
Figure 7: Reconstructed dE/dx versus momentum for different particle species. The thick black lines show the electron acceptance bands and momentum intervals for only dE/dx-based electron selection (for tracks without a match in TOF or EMC).
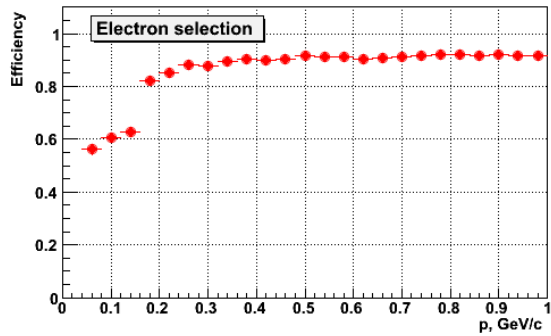
Figure 8: Electron selection efficiency versus momentum.
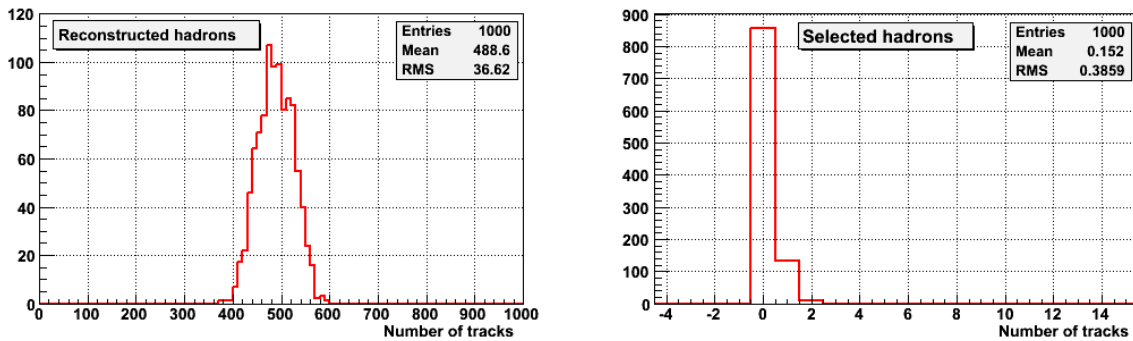
Figure 9: Number of reconstructed (left) and selected (right) hadron tracks. The overall (momentum integrated) hadron rejection factor is ∼3200.

9
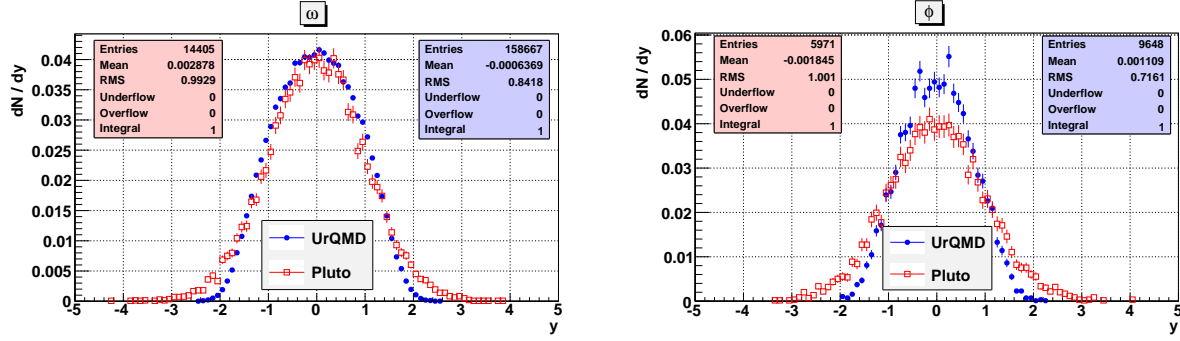
Figure 10: Rapidity distributions of ω and ϕ mesons obtained from Pluto and UrQMD generators in central (0-3 fm) gold-gold collisions at 7 AGeV.
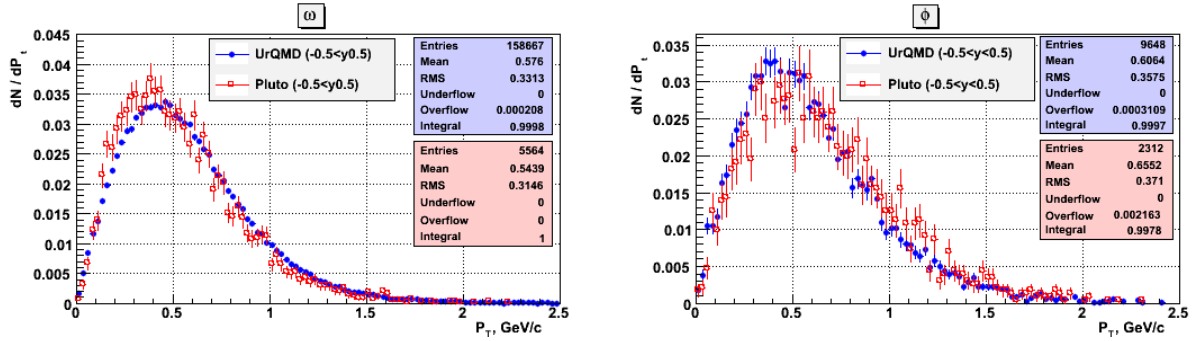
Figure 11: Transverse momentum distributions of ω and ϕ mesons obtained from Pluto and UrQMD generators in central (0-3 fm) gold-gold collisions at 7 AGeV.
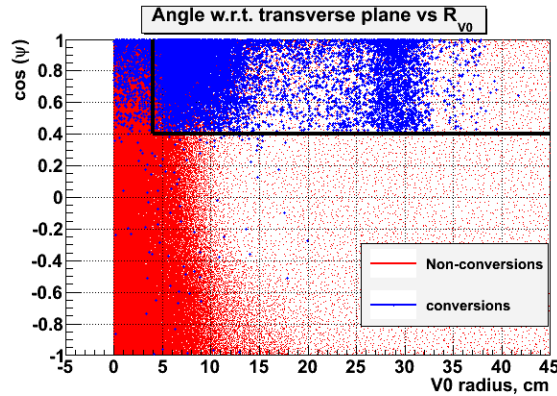
Figure 12: Cosine of the angle between the normal to the plane, defined by the electron-positron pair, and the magnetic field direction versus reconstructed radial position of the pair origin: blue points represent conversion pairs, red ones - the others. The rectangular region represents the conversion rejection cut.
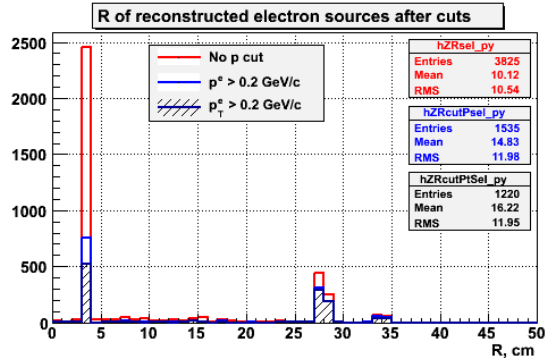
Figure 13: True radial positions of photon conversion points, giving reconstructed electron or positron (or both) after the topological cut was applied (Fig. 12). A low-p or low-p_T cut helps to reject conversion tracks.
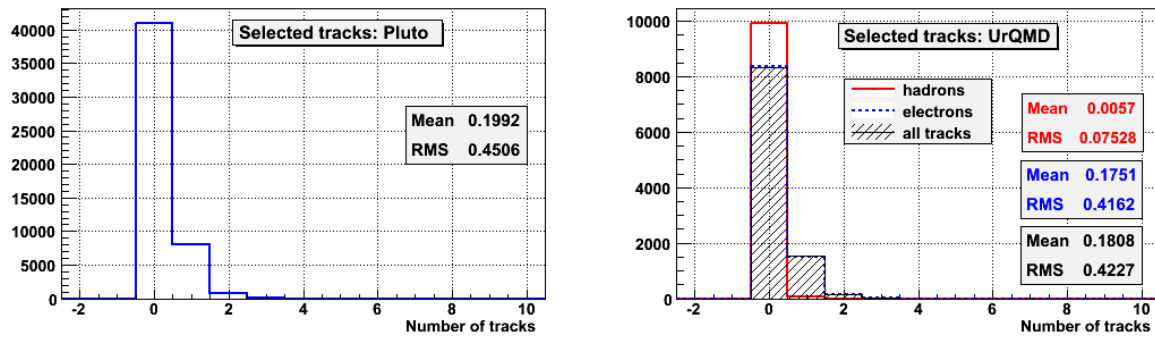
Figure 14: Track multiplicity distributions after final selection: left) signal (electrons/positrons from Pluto); right) background (electrons/positrons, hadrons and all tracks from UrQMD).
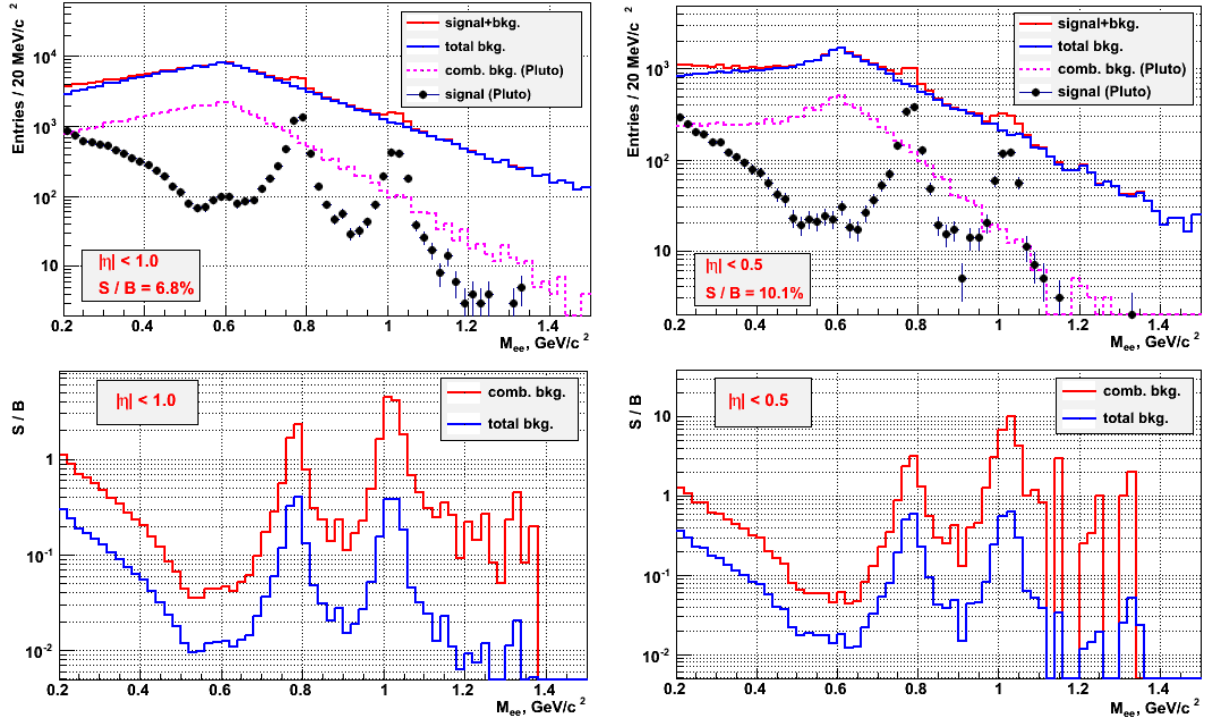
Figure 15: Reconstructed invariant mass of electron-positron pairs and signal-to-background ratios in invariant mass bins. Also shown are the integrated signal-to-background ratios for invariant mass values of 0.2-1.5 GeV/c^2.
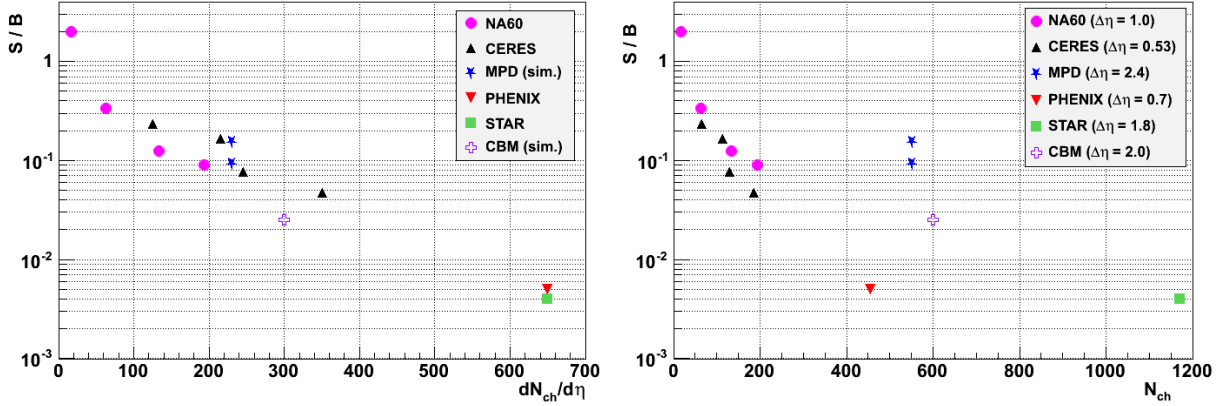
Figure 16: Signal-to-background ratios obtained in different experiments: left) versus charged particle density (per pseudorapidity unit), right) versus number of charged particles in the detector acceptance. The data shown are taken from [4–7] (CERES), [8] (NA60), [9] (PHENIX), [10] STAR, [16] (CBM) and the 4th row of Table 1 of this paper (MPD). Simulated results (CBM, MPD) do not include in-medium effects.